Robotic Exoskeletons for Upper Extremity Rehabilitation

Abhishek Gupta and Marcia K. O'Malley
Rice UniversityDepartment of Mechanical Engineering and Materials Science
Houston, Texas 77005 USA

1. Introduction

In 2003, 700,000 persons in the United States suffered a cerebral vascular accident (CVA), or stroke, with the total number of survivors estimated at 5.5 million. The total cost for rehabilitation and lost revenue in 2006 was 57.9 billion (Thom, Haase et al. 2006). Stroke commonly causes significant residual physical, cognitive, and psychological impairment (Gresham 1990). As the geriatric population increases and more effective therapies for acute stroke management emerge, there will be more survivors living with disabilities. In addition to greater numbers of survivors, there has been an increase in the number of more moderately affected survivors (Wolf, D'Agostino et al. 1992), which has increased the demand for stroke rehabilitation in an era of health care cost containment. Efforts to prevent stroke must, therefore, be balanced with pragmatic efforts to prevent disability and maximize quality of life for stroke survivors. Persons with hemiparesis following stroke constitute the largest group of patients receiving rehabilitation services in this country. The current consensus regarding rehabilitation of patients with some voluntary control over movements of the paretic limb is that they be encouraged to use the limb in functional tasks and receive training directed toward improving strength and motor control, relearning sensorimotor relationships, and improving functional performance (Gresham, Alexander et al. 1997). Given such recommendations, the research community has responded with efforts to improve the effectiveness of rehabilitative treatment of motor disability resulting from stroke.

1.1 Robotic devices for rehabilitation

A significant area of focus has been on the use of robotic devices for delivery of consistent and repeatable movement therapy. Indeed, the interest in rehabilitation applications for robotic devices, especially simple one- and two- DOF devices that focus on upper-extremity rehabilitation, has been increasing since the late 1980s and early 1990s (Erlandson 1992;

Reinkensmeyer, Dewald et al. 1996; Reinkensmeyer, Takahashi et al. 2000). For example, Khalili and Zomlefer suggested that a two joint robot system could be used for continuous passive motion and could be programmed to the particular needs of the patient (Khalili and Zomlefer 1988). Goodall et al. used two single degree-of-freedom (DOF) arms to stabilize sway in hemiparetic patients, and suggested the level of assistance could be withdrawn to encourage patients to relearn to balance on their own (Goodall, Pratt et al. 1987). White et al. built a single DOF pneumatically powered orthotic device for elbow flexion that could be used for continuous passive motion, to measure patient strength, and to assist elbow flexion (White, Scneider et al. 1993). Dirette et al. showed that a continuous passive motion (CPM) machine, when used regularly, can effectively reduce edema in the hands of flaccid hemiparetic patients (Dirette and Hinojosa 1994).

A more recent thrust of robotic assisted rehabilitation research has been to focus on the ability of the devices to assist limb movements and facilitate recovery of motor function in subjects with chronic hemiparesis due to stroke, such as with the Mirror-Image Motion Enabler – MIME (Burgar, Lum et al. 2000). In an initial study with MIME including twenty-eight subjects (two groups of 14), all had improved motor function as a result of therapy (Burgar, Lum et al. 2000). Preliminary data from these ongoing clinical efficacy trials suggest that robot-aided therapy has therapeutic benefits. Improvements have been demonstrated in strength and in the Fugl-Meyer (FM) assessment of motor function. Trends in the data suggest that the underlying mechanisms for these results may be increased strength, as well as more appropriate activation and inhibition of muscle groups.

The reader is referred to extensive reviews of robotic therapy for upper and lower extremity for a more complete discussion of the state of the field and results of ongoing clinical trials (Fasoli, Krebs et al. 2004; Hogan and Krebs 2004; Reinkensmeyer, Emken et al. 2004; Stein 2004; Riener, Nef et al. 2005; O'Malley, Ro et al. 2006). The MIME studies together with the cited related work support the conclusions that robotic manipulation of an impaired limb may favorably affect recovery following a stroke. An important additional finding is that improvements in motor control are possible beyond six months following a stroke.

Such findings with shoulder and elbow rehabilitation motivate the extension of robotic-assisted rehabilitation distally for the upper extremity, so that forearm pronation-supination, wrist flexion-extension, radial-ulnar deviation, and ultimately digital manipulation are enabled. Several devices have been presented in the literature to achieve at least a subset of these movements. For example, Charles et al. (Charles 2005) have developed an extension of the MIT-MANUS system to provide three rotational degrees-of-freedom for wrist rehabilitation. Hesse et al. (Hesse, Schulte-Tigges et al. 2003) have also extended the utility of their arm trainer to include wrist motion. In order to improve the applicability of the MIME system for full arm rehabilitation post stroke, the authors have developed a wrist rehabilitation robot, the *RiceWrist*, which interfaces with MIME and provides a variety of interaction modes for the therapist to select for the patient.

1.2 Haptic interfaces

Haptic or force-reflecting interfaces are a specific type of robotic device used to display touch- or force-related sensory information from a virtual or remote environment to the user (see, for example, surveys (Boman 1995; Burdea 1996; Lay and Day 2003). The ability to interact mechanically with virtual objects through incorporation of haptic feedback allows users to manipulate objects in the simulated or remote environment with ease when compared to a purely visual display. Added advantages of haptic simulators include

increased repeatability, scalability, safety, and control over environmental conditions. It is also possible to simulate additional physical forces and fields, which may or may not be part of a natural environment, to convey information to the user. This makes a haptic display suitable for a variety of applications like remote operation in hazardous environments, simulators for surgical training (Basdogan, Ho et al. 2001; Feygin, Keehner et al. 2002; Carignan and Akin 2003), and rehabilitation research (Todorov, Shadmehr et al. 1997; Prisco, Avizzano et al. 1998; Jack, Boian et al. 2001; Sveistrup 2004). Physical therapy utilizing the resistance offered to a user's motion during haptic interaction can be used for rehabilitation of impaired arm movements in patients. Furthermore, research has shown that augmented feedback presented in virtual environments accelerates the learning of motor tasks (Todorov, Shadmehr et al. 1997). For these reasons, the authors have developed an arm exoskeleton that can be utilized for such training and rehabilitation applications.

1.3 Force feedback exoskeletons

In order to effectively interface with the distal joints of the upper extremity, many groups are turning towards exoskeleton-type robotic devices. Such ungrounded or wearable interfaces permit greater human movement during haptic interactions. However, the increased workspace for an ungrounded (Tsagarakis, Caldwell et al. 1999) device is achieved at the expense of design simplicity when compared to grounded (Bergamasco, Allotta et al. 1994) devices.

A force-feedback exoskeleton is a haptic device worn by the user. Arm exoskeletons can simulate large forces at the hand or arm, like the weight of an object that is held. This is achieved by providing feedback to the various joints of the arm—the shoulder, elbow, and wrist. Although worn by the user, the device itself may be grounded, in which case it restricts user mobility. In the mid 1960s and early 1970s, a group of researchers at Cornell University and later at General Electric developed some of the earliest master-slave teleoperation systems, the Handyman and Hardiman (Mosher 1967). The Hardiman was an anthropomorphic exoskeleton placed inside a larger slave robot, and was used to amplify human power output. Input commands from the user were obtained from both the arms and legs. These early exoskeleton haptic devices were hampered by limitations in actuation, computation, and control systems technology. The reader is encouraged to review (Burdea 1996) for an exhaustive discussion of the early stages of exoskeleton and haptic interface development. In recent years, improvements in sensing and actuation technologies, control systems, and computing resources have led to the development of many successful haptic interfaces.

Although there have been a large number of high-performance hand controllers, research in design of exoskeletons for other parts of the body is still in an early phase. The first modern exoskeleton arm/glove was designed and developed at ARTS laboratory for the replication of sensations of contacts and collisions (Bergamasco, Allotta et al. 1994). The ARTS arm, also known as the PERCRO exoskeleton, is a 7-DOF ungrounded device, attached to the operator's shoulder and torso. The operator holds onto the device with his/her palm. Hence, the device can only exert forces at the palm of the user. It uses DC motors with a cable transmission system for actuation. A 9-DOF under-actuated exoskeleton arm developed at the Korea Institute of Science and Technology (KIST) by Lee et al. addressed the workspace issues associated with the PERCRO exoskeleton. Their device allows for full reproduction of the human arm's workspace when operating the exoskeleton (Lee, Park et al. 1998). A revised exoskeleton device from the same group employs electrical brakes in place of pneumatic actuators for improved bandwidth (Kim, Lee et al. 2005). An alternate arm exoskeleton developed at KIST addresses the limited wearability issues of previous designs by using parallel mechanisms and pneumatic actuators (Jeong, Lee et

al. 2001). The wearable Salford arm addresses some of the issues and limitations of earlier designs (Tsagarakis, Caldwell et al. 1999). For example, nearly 90% of the human arm's workspace can be replicated with their device. Pneumatic muscle actuators (pMAs) were selected to power the robot due to their high power-to-weight ratio. A drawback of this choice is the highly nonlinear behavior and slow response of the pMAs, presenting additional control challenges.

In recent years, robotic exoskeletons are being developed specifically for rehabilitation applications, such as the ARMin system. This six-DOF device was designed to enable training for specific activities of daily living (Nef, Mihelj et al. 2006). Kousidou et al. have incorporated the Salford arm into the Rehab Lab system for virtual rehabilitation of complex three-dimensional trajectories in the workspace (Kousidou, Tsagarakis et al. 2006). Carignan et al. (Carignan and Liszka 2005) present a prototype five-DOF exoskeleton system currently under development that focuses on shoulder rehabilitation. Finally, Gupta et al. have incorporated their lower-arm exoskeleton device (Gupta and O'Malley 2006) into the MIME system, creating a full upper-extremity robotic rehabilitation system (Gupta, Patoglu et al. 2007). A review of exoskeleton devices for rehabilitation applications was compiled by Ruiz et al., and contains images of many of these devices (Ruiz, Forner-Cordero et al. 2006).

1.4 Exoskeleton control

Force control of arm exoskeletons is traditionally implemented under the assumption of pseudostatic operation (see, for example, (Bergamasco, Allotta et al. 1994)). In this approach, the robot Jacobian can be used to compute required actuator torques for some desired force at the end-effector. Recently, Rosen et al. presented some interesting results with the use of myosignals, command signals sent to the human muscles by the brain, in predicting human arm motion during operation of a single-DOF arm exoskeleton (Rosen, Brand et al. 2001). They demonstrated that the prediction of operator motion can be used to improve upon the force control and overall quality of the haptic device. The group has since expanded their design to include the full seven-DOF of the arm (Perry and Rosen 2006).

1.5 Exoskeleton design

Many exoskeleton interfaces attempt to optimize one or more of the following characteristics of the haptic system, namely power-to-weight ratio (Lee, Park et al. 1998; Tsagarakis, Caldwell et al. 1999; Jeong, Lee et al. 2001), workspace (Lee, Park et al. 1998), wearability (Jeong, Lee et al. 2001) or stability, and control bandwidth (Bergamasco, Allotta et al. 1994; Nakai, Oshashi et al. 1998; Williams II 1998). Individual designs, however, achieve these optimizations at the expense of other useful features, usually workspace (Bergamasco, Allotta et al. 1994; Nakai, Oshashi et al. 1998; Jeong, Lee et al. 2001) or control bandwidth (Lee, Park et al. 1998; Tsagarakis, Caldwell et al. 1999; Jeong, Lee et al. 2001). In this chapter, the authors present work towards the design of a high-quality haptic interface with a workspace comparable to that of human arm workspace. This is achieved at the expense of added weight and decreased mobility due to device grounding.

2. Design Challenges

Haptic feedback aids an operator to reliably complete a remote or virtual task. Primary requirements for such a system are the ability to convey commands to the remote or virtual plant and to reflect relevant sensory information, specifically forces in the remote or virtual environment, back to the operator. In essence, the dynamics of the device must not

interfere with the interaction between the operator and environment. An ideal haptic interface behaves as a rigid body, through which the user interacts with the environment, over the complete range of frequencies of forces in the virtual environment.

In practice, however, performance is limited by physical factors, such as actuator and sensor quality, device stiffness, friction, device workspace, force isotropy across the workspace, backlash, and computational speed. Force isotropy, which refers to the equality of force exertion capability of the device in all directions, is important to ensure consistent device performance across the workspace. The desired size and shape of the workspace itself is typically dependent on the target application, and serves as an important factor in determining the overall device size and mechanism. Increased workspace is only achieved at the expense of a larger and heavier device, since the force output requirements scale with the workspace size. Also of consideration in the design of haptic arm exoskeletons is the biomechanics of the human arm. The arm imposes a force/position constraint on the device, thus affecting the system behavior and performance. These design factors are discussed in detail in the following sections.

2.1 Biomechanics of Human Arm

A haptic arm exoskeleton places kinematic constraints on the human arm. The human arm has seven DOF: abduction/adduction and flexion/extension of the shoulder; rotation of the upper arm; flexion/extension of the elbow; rotation of the forearm; and radial/ulnar deviation and flexion/extension of the wrist. It is desirable that the haptic exoskeleton does not compromise the natural arm motion and workspace of the operator. The device should also have torque capabilities to match and enhance human abilities. Table I shows the workspace and torque capabilities of the human arm for reference.

2.2 Performance-Related Design Parameters

A high-quality haptic interface is characterized by stability robustness and transparency. The stability bandwidth refers to the range of frequencies of forces that can be reflected to the operator with the device, while ensuring stable system behavior. Research has shown that stability of a haptic simulation is related to the simulation rate, virtual wall stiffness, and device viscosity (Elllis, Ismaeil et al. 1996). Transparency is a measure of the degree of distortion between the force at the human-robot interface and the desired contact force as commanded through the virtual environment. Transparency can be degraded by such things as backlash, inertia, or friction in the haptic device, sensor resolution, and computational delay (Colgate and Brown 1994). Often with haptic interfaces, the quality of the device is characterized by the maximum virtual wall stiffness that can be stably displayed.

Joint	Human Isometric Strength (Nm)	Human Joint Workspace Limits (degrees)
Elbow Flexion/Extension	72.5	Flexion: 146 Extension: 0
Forearm Supination/Pronation	9.1	Supination: 86 Pronation: 71
Wrist Palmer/Dorsal Flexion	19.8	Palmer Flexion: 73 Dorsiflexion: 71
Wrist Abduction/Adduction	20.8	Adduction: 33 Abduction: 19

Table 1. Workspace and torque limits of human arm.

Research has shown that fairly low stiffness and force values are sufficient for object detection (O'Malley and Goldfarb 2002; O'Malley and Goldfarb 2004). Therefore, if a haptic exoskeleton is designed for teaching arm movements using virtual force fields, a low force output interface would suffice. In this case, as the authors intend for the device to be used as a general purpose training tool for arm movements, it is required that the device be able to simulate high-quality virtual surfaces. As a result, emphasis is placed on the design of a high-performance interface, which encompasses the human arm workspace. In addition, for rehabilitation applications, the ability to control feedback to individual human arm joints is desirable and has been addressed through this design.

2.3. Control-Related Design Parameters

As mentioned earlier, a haptic system applies trajectory-dependent forces to the operator's body. This is typically implemented in one of two modes—the impedance control mode or the admittance control mode. Impedance control techniques measure position at the human-machine interface and in turn adjust the commanded force at the human-machine interface depending on the virtual environment model to be displayed. It is desirable that an impedance-controlled haptic device allows free movement in response to the operator's motion commands, so that when the human is moving in free space (not in contact with any virtual objects), there is no resistance to motion. This requirement translates to a need for backdrivability in impendence-controlled haptic devices. In this control mode, it is also desirable for the device to have minimal inertia to facilitate maneuvering. Furthermore, low inertia and friction improve interface performance by reducing the forces required to compensate for device dynamics. Alternatively, admittance control methods rely on measurement of forces at the human-machine interface and controlled robot motion based on the virtual environment model. An admittance controlled haptic device should prevent movement of the robot in response to operator-generated forces to allow for consistent force measurement and motion control.

It is apparent that haptic exoskeleton design involves various tradeoffs, which limit the achievable performance of the device since, in all instances, stability must be maintained. To summarize these tradeoffs, mechanism design choices may limit or affect human motion abilities; sensor and actuator selection is directly related to device weight, force output range, system stability, and cost; and actuator placement and inclusion of transmissions affects the apparent inertia of the device. All of these design decisions are greatly influenced by the intended application for the device.

The MAHI exoskeleton, named for the Mechatronics and Haptic Interfaces Lab at Rice University, has been designed primarily for training and rehabilitation in virtual environments. These applications typically require the use of virtual force fields for guidance (Rosenberg 1993) or active assistance (Gillespie, O'Modhrain et al. 1998; O'Malley and Gupta 2003). The exoskeleton device must therefore allow natural human arm movements, with minimal reduction in workspace of the human arm. Because the device is to be worn, special care must be taken to ensure safety of the wearer. Furthermore, mobility of the interface is not normally a requirement for such a system. Hence, the device can be grounded to support excessive weight, and gravity compensation can be implemented through the controller. Additionally, the low accelerations and velocities associated with human movements ensure that the inertia of the device plays a small role in its operation (Shimoga 1992; Bergamasco, Allotta et al. 1994). Therefore, when designing the MAHI exoskeleton, the kinematic design of the robot was given prime consideration.

3. MAHI arm exoskeleton

3.1 Basic Mechanism Design

The basic kinematic structure of the 5-DOF MAHI exoskeleton is depicted in Fig. 1. The exoskeleton is comprised of a revolute joint at the elbow, a revolute joint for forearm rotation, and a 3-revolute-prismatic-spherical (RPS) serial-in-parallel wrist.

The 3-RPS platform, mentioned by Lee and Shah (Lee and Shah 1988), consists of a base plate, three extensible links l_1, l_2, and l_3, and a moving platform, as shown in Fig. 2. The moving platform houses the end-effector that is affixed to the operator during operation. The moving platform is connected to the three extensible links by means of spherical joints spaced at 120° along the circumference of a circle of radius r. The other end of the links connects to the base platform via revolute (pin) joints, which are also spaced 120° along a circle of radius R. The axes of rotation of the revolute joints are oriented along the tangents to the circle of radius R. Linear actuators placed along the link are used to change the link length, thereby moving the top platform. It should be noted that the platform has limited movement transverse to the vertical axis through the base and no singularities for $\theta_i \in (0, \pi)$ (Lee and Shah 1988).

The choice of a parallel mechanism for the design of the exoskeleton wrist over a serial mechanism was motivated primarily by the compactness of the parallel mechanism. Furthermore, use of a parallel mechanism allows for higher torque output, stiffness, and decreased inertia compared to a similar serial mechanism. During operation, the robot is worn so that the axis elbow joint of the robot aligns with the operator's elbow joint, and the top plate of the wrist of the robot aligns with the wrist joint of the operator. This configuration aids in preserving natural arm movements by aligning the robot's kinematic structure with that of the human arm. Velcro strapping and an ergonomic palm splint are used to maintain this alignment. The mapping between the robot configuration and arm position is further simplified by the use of the 3-RPS kinematic structure for the robot. The equivalence between the human wrist joint angles and the xyz Euler angle representation for the orientation of the platform is shown in Section 3.4.
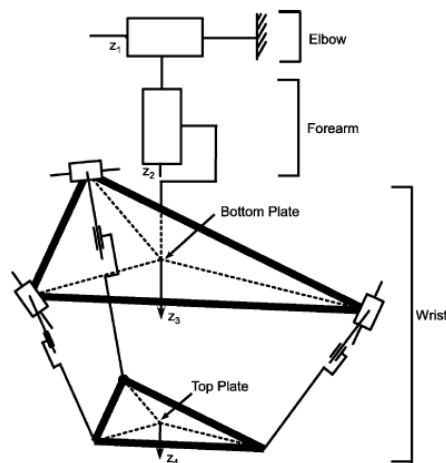

Fig. 1. Exoskeleton mechanism: A 3-RPS platform is used as the wrist of the robot. Joints R1, R2, and R3 and B1, B2, and B3 are located at vertices of equilateral triangles.
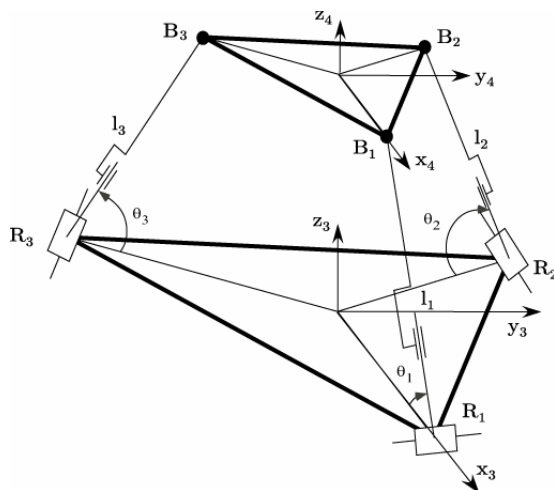
Fig. 2. 3-RPS platform, adapted from (Lee and Shah 1988).

3.2 Sensing and Actuation

Sensor Selection Sensor resolution affects the range of frequencies of forces that can be displayed by the haptic interface (Colgate and Brown 1994). Consider, for example, the simulation of a thin virtual wall. If the sensor resolution or the computational speed is not high enough, then there exists a possibility that the human can pass his/her arm through the wall without feeling the force. Furthermore, during simulation of stiff virtual surfaces, reduction in sensor resolution increases the delay in sensing the human's actions in the virtual environment, and this delay can decrease system stability. With these considerations, high resolution optical encoders were selected for the device.

Actuator Selection The actuators for a haptic device determine the range of magnitude and frequencies of forces that can be displayed with the interface. To reproduce real-life environments, it is desirable that the device be able to display forces in a large range of magnitudes as well as frequencies. In general, the use of high-power actuators is accompanied with an increase in weight, thereby increasing the inertia of the device. Thus, high power-to-weight ratio and high bandwidth are desirable qualities for actuators used in a haptic interface. The bandwidth refers to the dynamic response of the actuator; a low-bandwidth actuator fails to display high-frequency forces to the operator, reducing system transparency in such situations. This gains importance in that human kinesthetic/proprioceptive sensing bandwidth is 20-30 Hz and tactile sensing bandwidth is 0-400 Hz (Shimoga 1992).

No single actuator technology provides the benefit of both high power-to-weight ratio and high bandwidth. Pneumatic actuators are inexpensive and provide the benefit of high power-to-weight ratio. However, pneumatic actuators have a low bandwidth, which limits their utility as actuators for haptic interfaces. Tsagarakis et al. used pMAs for their exoskeleton (Tsagarakis, Caldwell et al. 1999). However, these actuators have highly nonlinear dynamics in addition to low bandwidth, making them unsuitable for application in haptic devices. Hence, electrical actuation was chosen for the MAHI exoskeleton. Electrical actuators have a lower power-to-weight ratio than pneumatic actuators but have

very high bandwidth. This increases the weight of the device but allows for better force reflection through the interface.

Transmission and Actuator Placement A transmission can be used to increase the torques or forces delivered by the device, but at the expense of speed of operation. The bandwidth of human motor output, which represents the ability of the hand and fingers to exert forces, is 10-15 Hz (Shimoga 1992), thus making the use of a transmission in haptic interfaces advantageous. Furthermore, use of a transmission allows the actuators themselves to be placed closer to the base of the robot, reducing rotational inertia. Use of transmissions, however, is associated with tradeoffs like backlash, nonlinear dynamics, and complex cable routing. For example, gears introduce backlash into the system, whereas belt drives introduce nonlinearities. Friction, backlash, backdrivability, and size were key considerations in designing the transmission. A cable drive, which, by design is backdriveable and free of backlash, is used as the transmission for elbow and wrist. In contrast, the forearm joint is direct drive actuated. For the elbow joint, a large cable drive with an approximate 10:1 transmission ratio was used, allowing backlash-free motion that is fully backdriveable (See Fig.3). High torque rotary electric motors with a cable-driven mechanism are employed for the robot wrist (Fig. 4), whereas the forearm joint is directly driven using a frameless electrical motor.
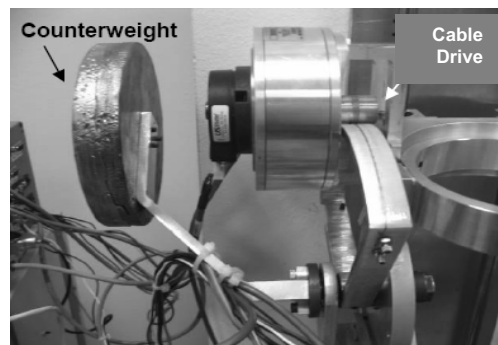

Fig. 3. Elbow joint with a cable drive and counterweight for gravity compensation.

Fig 4. Wrist component of the MAHI arm exoskeleton employing electrical motors with a cable drive.

Fig. 5. User operating the MAHI arm exoskeleton.

3.3 Mechanical Design of MAHI Exoskeleton

Fig. 5 depicts a user operating the MAHI arm exoskeleton. The forearm joint employs a frameless brushless DC motor with direct actuation. Due to the use of frameless actuators, the amount of material required for construction was minimized thus reducing the weight of the device. The wrist platform is actuated through high torque rotary electric motors and a cable drive transmission. The range of motion of the spherical joint at the movable plate of the platform limits the workspace of platform. Equations developed by Lee and Shah were used to compute the range of rotations required from the spherical joint in order to meet our workspace criteria (Lee and Shah 1988). It was found that commercially available spherical joints do not suffice to meet the workspace requirements. Hence, the spherical joint was replaced by a 4 DOF spherical joint between the top plate of the platform and the corresponding linear joint links. This joint consisted of a universal-joint attached at either end to the link and the moving platform via rotary joints. This adds redundancy to the system and permits larger rotations. For the purpose of kinematic analysis, the redundancy does not affect any of the geometric relations or equations. Mechanical stops at workspace limits, soft software stops and an emergency stop switch are employed to ensure operator safety. For a detailed discussion of the design of the exoskeleton, the reader is referred to (Gupta and O'Malley 2006; Sledd and O'Malley 2006).

3.4 Kinematic Properties of MAHI Arm Exoskeleton

Table 2 shows the workspace for the MAHI arm exoskeleton in terms of the range of motion about each of the three primary degrees of freedom and corresponding human joint workspace limits. The device is singularity-free and the forward and kinematics of the device have a unique solution within the workspace. For a detailed discussion of the kinematics of the robot refer to (Gupta and O'Malley 2006).

Joint	Peak Torque Output Limits (Nm)	Joint Workspace Limits (degrees)
Elbow Flexion/Extension	55	Flexion: 90 Extension: 0
Forearm Supination/Pronation	5.08	Supination: 90 Pronation: 90
Wrist Palmer/Dorsal Flexion	5.26	Palmer Flexion: 45 Dorsiflexion: 45
Wrist Abduction/Adduction	5.26	Adduction: 45 Abduction: 45

Table 2. Workspace and torque output limits of MAHI arm exoskeleton.

The workspace of the MAHI arm exoskeleton is 100% of the average human joint range of motion except for palmar flexion and dorsiflexion where it is 60%. As shown in Fig. 6, compound movements of the wrist remain singularity-free, albeit with some reduction in the range of motion similar to the case of a human wrist. Thus the MAHI arm exoskeleton provides adequate range of motion for a human operator. It should also be noted that the device is backlash- free due to the use of direct-drive and cable-driven actuation and is highly backdriveable. Furthermore, the 3-RPS platform allows for compact design, centered on the human arm, which increases wearability and maximizes the achievable workspace of the exoskeleton.
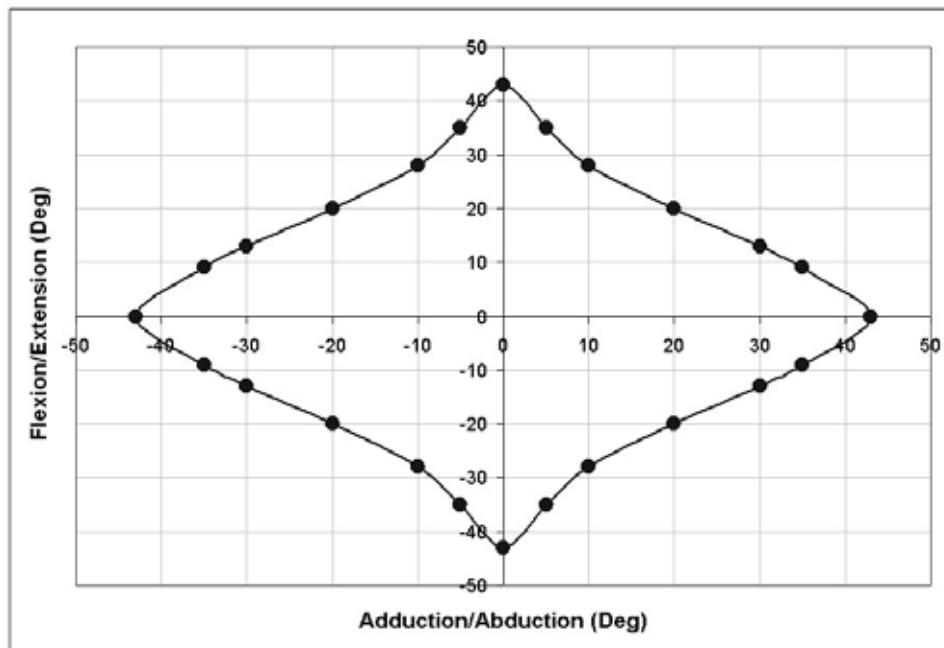

Fig. 6. Range of motion of MAHI arm exoskeleton wrist.

Fig. 7 shows the manipulability of the MAHI arm exoskeleton measured as the absolute determinant of the inverse Jacobian (Yoshikawa 1985). Manipulability of a robot is a quantitative measure that captures the ease with which the device can arbitrarily change

position and orientation from a given posture. For the MAHI arm exoskeleton, the manipulability measure is greatest in the center of the workspace, with the wrist at 0° of abduction/adduction, (a) and flexion/extension, (b). Manipulability, as expected, is low at the extents of each joint range of motion, although more so during flexion/extension. For the tasks of rehabilitation and training, it is expected that most useful interactions via the haptic device will take place away from the joint limits, and so manipulability should not limit device performance.

Measurement of Human Motion A simplified kinematic model of the human lower arm and the wrist is shown in Fig. 8. Notice that axes x_4 of the platform (see Fig. 2) and z_2 of the human wrist joint coincide when the exoskeleton is worn by an operator. Similarly, axes y_4 of the platform and z_3 of the arm coincide for any rotation, α, of the top plate of the platform about x_4, or of the human wrist about z_2 (Fig. 8). Furthermore, {3} of the platform has a fixed orientation with respect to {1} of the human arm.
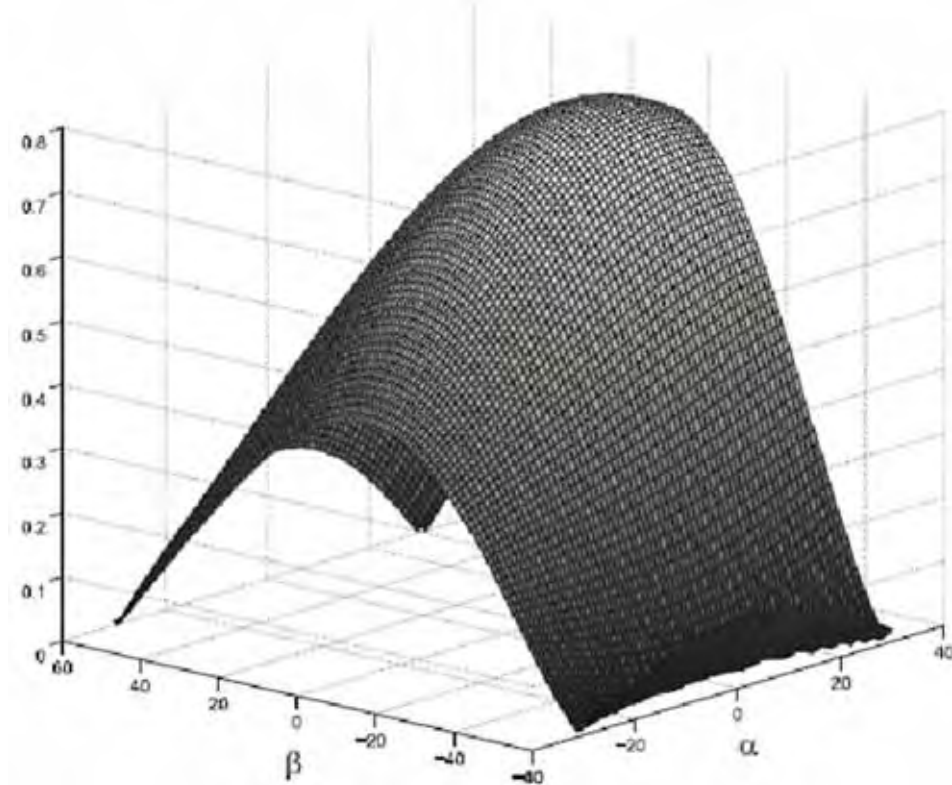

Fig. 7. Manipulability of the wrist mechanism.

Hence, a rotation of the top plate of the platform about axis x_4 (Fig. 2) followed by another rotation about axis y_4 (Fig. 2), is equivalent to a transformation from {3} to {1} of the arm. This implies that with the top plate of the platform centered at the operator's wrist joint, the measurement of the orientation of the top plate with respect to the base of the platform in terms of xyz-Euler angles corresponds to measurement of the flexion/extension and

abduction/adduction of the human wrist joint. Thus, the Euler angle of rotation α about axis x_4 corresponds to abduction/adduction of the wrist while the rotation angle β about y_4 corresponds to flexion/extension. With the forearm joints of the robot and human being coincident, the measurement of position of operator's elbow and forearm from robot coordinates and vice versa is trivial.
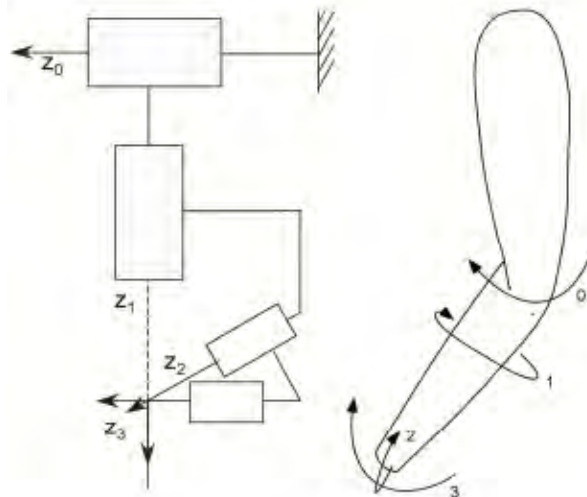

Fig. 8. Simplified kinematic model of the human arm: Other axes have not been shown for clarity. Axes 0 through 3 represent elbow rotation, forearm rotation, wrist adduction/abduction and wrist flexion/extension respectively.

4. Control and Dynamic Performance

The MAHI arm exoskeleton is controlled via a 3.2 GHz Pentium 4 PC with 2GB of RAM. The hardware is controlled through the MATLAB Real Time Workshop Toolbox from Mathworks, and WinCon from Quanser Consulting. All data I/O is handled by the Q8 board from Quanser. Position and force controllers were designed for the elbow, forearm and the wrist platform. Separate joint-space and task-space controllers were designed and tested for the wrist platform. Note that the task-space of the wrist platform refers to the three degrees of freedom corresponding to flexion/extension and abduction/adduction of the wrist, and the height of the platform. The following sections describe controller design in detail.

4.1 Controller Implementations
Joint level control for the MAHI exoskeleton is implemented via a joint-space proportional derivative (PD) trajectory controller. In addition, an inverse kinematics based task-space position controller was designed for the wrist, as shown in Figure 9. The commanded task-space positions and velocities were used to generate reference commands for the aforementioned joint-space controller. The performance of the device under joint-space position control was verified through step responses, set joint control and trajectory following control.

A task-space PD position controller for the wrist platform was also implemented as shown in Figure 10. As compared to the inverse kinematics based controller described in the previous section, this controller allows for independent control of wrist degrees of freedom, namely abduction/adduction, flexion/extension, and platform height. This is critical as during operation it is desirable to constrain the height of the platform to be a constant dependent upon the length of the subject's forearm. Furthermore, this provides the ability to selectively provide guidance and/or feedback to individual human wrist joints. The performance of the controller is discussed in Section 4.2.

Force control for the exoskeleton is implemented as a task-space impedance force controller, as shown in Fig. 10. It is assumed that the velocities of motion are small enough to ignore the dynamic terms in the equations of motion of the device. It should be noted that in the case of the elbow and forearm, the task-space and the joint-space are the same and hence, the impedance controller is simply a joint-space controller. The results of force control are discussed in Section 4.2 through haptic display of virtual walls.
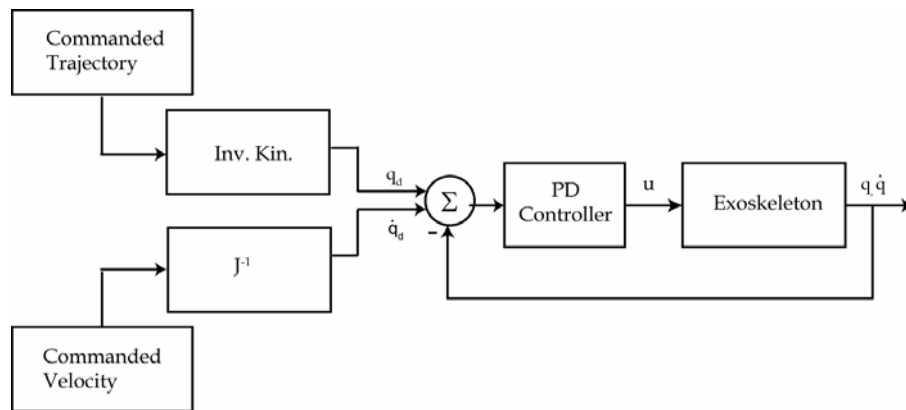

Fig. 9. Inverse kinematics based trajectory controller for the MAHI Exoskeleton where, J is the Jacobian of the device; q_d, $\dot{q}_d$ are the desired joint position and velocities; q, $\dot{q}$ are the current joint position and velocities; and u is the control input.

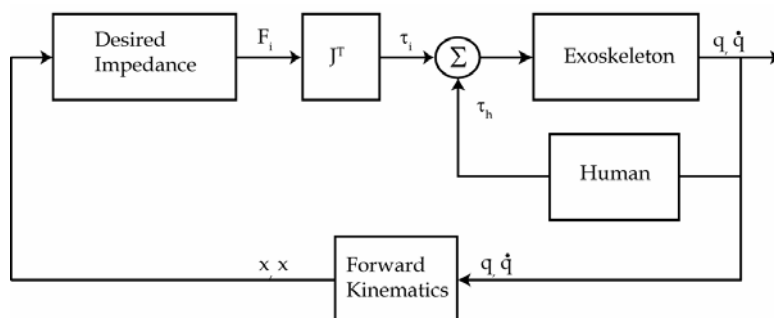Fig. 10. Task-space impedance controller for the MAHI arm exoskeleton, where, q, $\dot{q}$ are the current joint position and velocities; x, $\dot{x}$ are the current task-space position and velocities; F_i is the desired environment force; J is the Jacobian of the MAHI exoskeleton; τ_i is the desired joint torques; and F_h is the human induced joint torque.

4.2 Dynamic Performance

Tables 1 and 2 list the human isometric strength and the peak torque output capabilities of the MAHI arm exoskeleton for the corresponding joints, respectively. The torque capabilities lag behind human abilities due to practical considerations owing to the power-to-weight characteristics of electrical actuators. Coulomb friction was measured to be 0.041 Nm and 1.134 Nm in the forearm and wrist joints respectively. Viscous friction was found to be negligible.

Position Control As described in Section 4.1, the position control for the wrist and forearm was implemented through a PD controller. Figure 11(a) shows the closed loop step response of the forearm. It can be easily seen that the device reaches steady state position of 1 rad in less than 1 s with no overshoot or oscillations. There is a small steady state error (< 1%) in position due to friction in the bearings, motor cogging and the gravitational torque acting on the joint. The steady state error can be eliminated with the use of a PID controller instead of the PD controller employed. The trajectory following behavior of the forearm tracking a sinusoidal reference signal at a frequency of 4 rad/s is depicted in Figure 11(b). This further verifies that the bandwidth of the controller is over 4 rad/s and matches human actuation bandwidth. Similar results were obtained for the wrist controller.

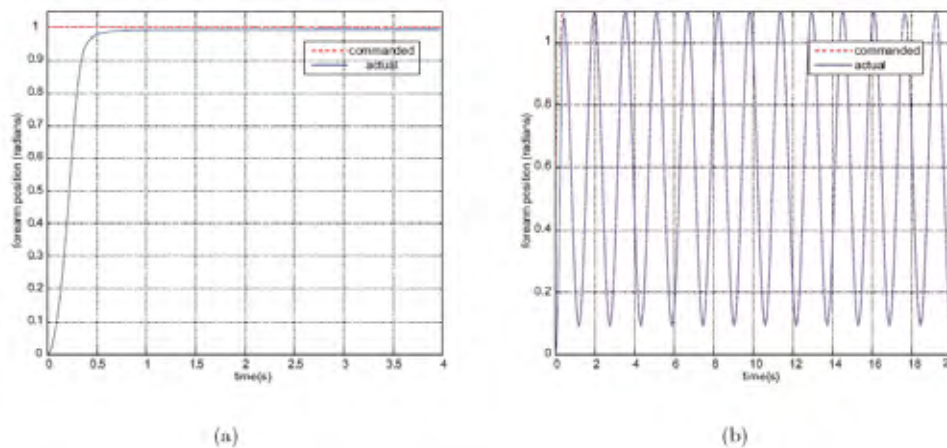(a)   (b)

Fig. 11. Position control of the forearm position controller: (a) Step response to a reference signal with a step of 1 rad shows no overshoot and quick, non-oscillatory response. (b) Trajectory following behavior when tracking a 4 rad/s sinusoidal reference signal of amplitude 0.5 rad centered at 0.6 rad demonstrates that the device bandwidth matches human capabilities.

Joint level position control for the wrist was implemented via independent PD controllers acting on each joint, as discussed in Section 4.1. Control results demonstrated that there is negligible structural coupling between the actuated joints. The low structural coupling between the linear joint axes also serves to verify the mechanical design process showing that the axes could be independently controlled as theoretically predicted. A task space PD controller for the wrist platform was also implemented as described in Section 4.1. Trajectory following behavior of the task-space controller tracking sinusoidal trajectories in abduction/adduction and flexion/extension at 4 rad/s is shown in Figure 12. Note the quick system response with little overshoot when tracking sinusoidal trajectories of

amplitude 0.15 rad at a frequency of 4 rad/s. Note that the platform height was constrained when testing responses in abduction/adduction and flexion/extension as we start at the boundary of the workspace where it is not possible to change orientation of the top plate of the platform without changing platform height. Trajectory following capability is useful for guidance during training or rehabilitation. These results also serve to verify adequate system performance throughout the workspace of the wrist. For a detailed discussion of the performance of the device under position control please refer to (Gupta, Patoglu et al. 2007).
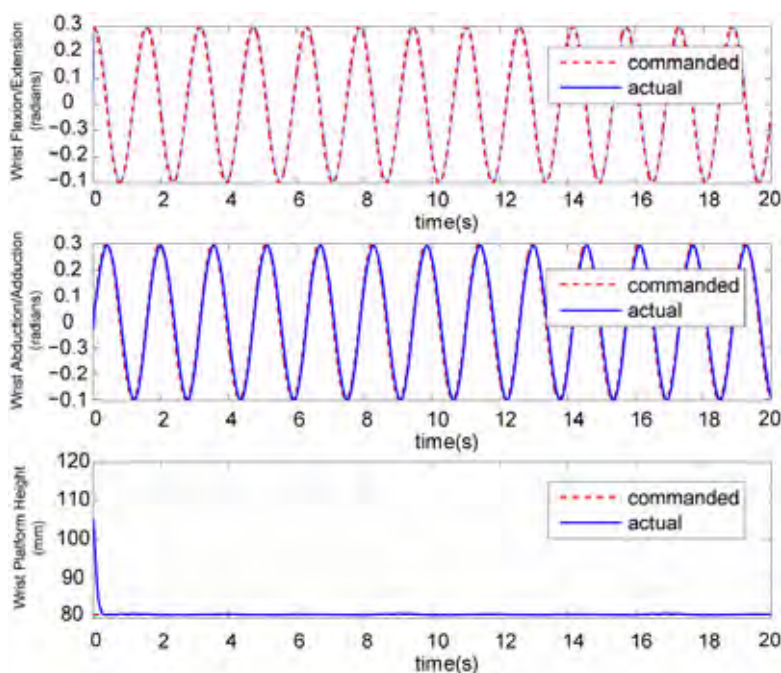

Fig. 12. Task space trajectory tracking control of the wrist platform (reference: height– 80 mm; abduction/adduction and flexion/extension – sinusoids of amplitude 1.5 rad at 4 rad/s).

Force Control As described in Section 4.1 force control for the exoskeleton was implemented through an impedance controller. Figure 13 depicts a subject's interaction with a virtual wall at the forearm joint, implemented as a spring-mass system of stiffness 150 Nm/rad and damping of 10 Nm/rad/s, located at 1 rad. Regions (a), (b) and (c) demonstrate the approach, steady contact and penetration into the wall, respectively. Note that due to torque limitations of the forearm motor, the user can overcome the wall force, thereby saturating the motor. Larger motor output is desired for simulating stronger walls, but device torques that exceed human limits could compromise user safety.

Figure 14 depicts a typical user interaction with two virtual walls located at a rotation of 0.2 rad in flexion/extension and abduction/adduction respectively. The virtual wall was implemented as a spring-damper system. Although slight chattering is noticed upon contact, the device successfully constrains the operator. Upon decreasing the wall gain, it is noted that chatter occurs at larger user penetration depths into the wall. The platform

torque output does not match the limits of the human joints and hence, the human operator can saturate the motor output. We believe this actuator saturation along with the low stiffness of the cable drive transmission to be responsible for the chatter.
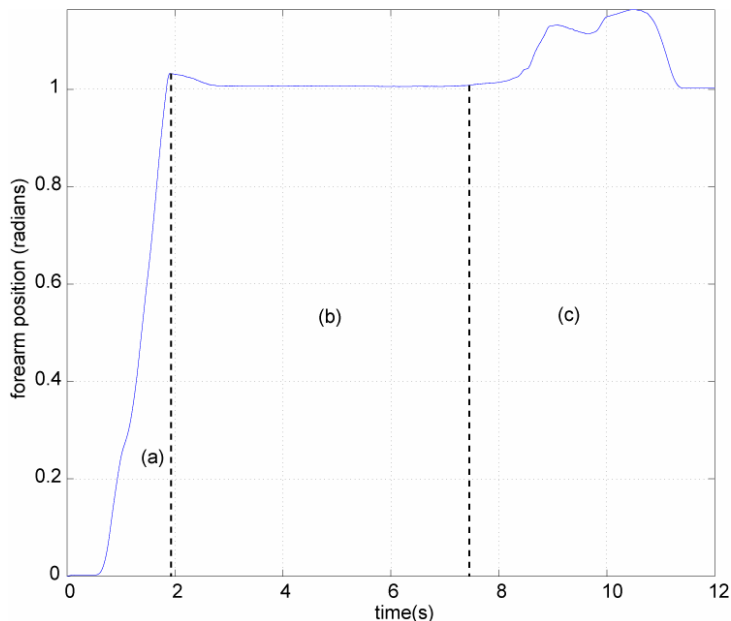

Fig 13. User interaction with virtual wall located at 1 rad for the forearm joint. Regions (a), (b) and (c) demonstrate the approach, steady contact and penetration into the wall. 0.5 mm from their initial position. This demonstrates that there is negligible structural coupling between the actuated joints. The low structural coupling between the linear joint axes also serves to verify the mechanical design process showing that the axes could be independently controlled as theoretically predicted.
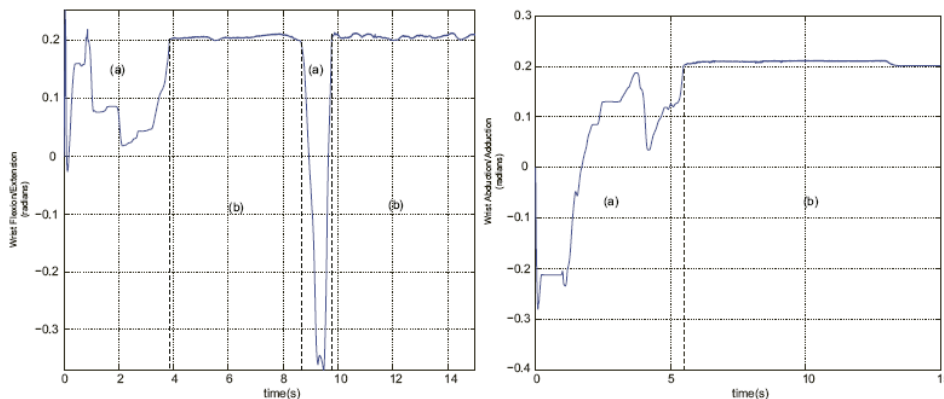

Fig. 14. (a) A virtual wall located at 0.2 rad wrist flexion/extension; (b) A virtual wall located at 0.2 rad wrist abduction/adduction.

5. Integration of MAHI exoskeleton with MIME

Prior work has studied the ability of a device (Mirror-Image Motion Enabler — MIME) (Burgar, Lum et al. 2000) to assist limb movements and facilitate recovery of motor function in subjects with chronic hemiparesis due to stroke. MIME incorporates an industrial robot and operates in three unilateral modes and one bimanual mode. In unilateral operation, passive, active-assisted, and guided movements against a resistance are possible. The bimanual mode enables the subject to practice bilateral, coordinated movements with rate and range under his or her control.

In the current version of MIME, subjects are seated in a wheelchair modified to improve seating support and reduce movements of the upper body. They can sit close to either the front or rear of an adjustable height table. A PUMA-560 robot is mounted beside the table. It is attached to a wrist-forearm orthosis (splint) via a 6-axis force transducer, a pneumatic breakaway overload sensor set to 20 Nm torque, and a quick-release coupling mechanism. The subject's arm is strapped into the splint with the wrist in neutral position. Robot/forearm interaction force and torque measurements from the transducer are recorded and archived by a personal computer. The control program monitors these data and the motion of the robot in order to prevent potentially hazardous situations from occurring. Switches and mechanical stops are strategically placed to permit rapid de-activation of the robot, if necessary.

Preliminary data from clinical efficacy trials using MIME suggest that robot-aided therapy has therapeutic benefits. Improvements have been demonstrated in strength and in the FM assessment of motor function. Trends in the data suggest that the underlying mechanisms for these results may be increased strength, as well as more appropriate activation and inhibition of muscle groups (Burgar, Lum et al. 2000).

Such findings with shoulder and elbow rehabilitation motivate the extension of robotic-assisted rehabilitation distally for the upper extremity, so that forearm pronation-supination, wrist flexion-extension, radial-ulnar deviation, and ultimately digital manipulation are enabled. The MAHI exoskeleton wrist (*RiceWrist*) has been integrated with the Mirror-Image Motion Enabler (MIME) (Burgar, Lum et al. 2000) system (see Figure 15). Velcro strapping and a molded splint are used to attach the subject's arm to the device. MIME and *RiceWrist* communicate through the serial port. Communication is mainly for synchronization of start and end of trials.

5.1 MIME-*RiceWrist* Rehabilitation Setup

Figure 16 shows the overall setup for the MIME-*RiceWrist* rehabilitation system. The therapist maintains high level supervisory control over the therapy session. The therapist can customize the physical therapy sessions according to the needs of individual patients. The *RiceWrist* extends the three unilateral operation modes of MIME to include forearm supination and pronation, wrist flexion and extension, and radial and ulnar deviation.

The three unilateral modes of MIME are:

- Passive mode: the robot guides the user to a predetermined goal position.
- Active-assisted mode: similar to passive mode, but the robotic assistance does not begin until the patient overcomes some preset force threshold.
- Constrained mode: the patient moves his/her arm against a viscous field to a goal position. A moving virtual wall prevents the patients from retracting their arm.
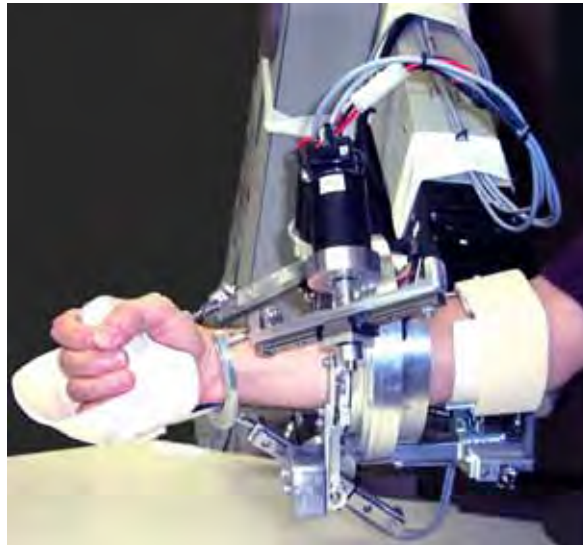
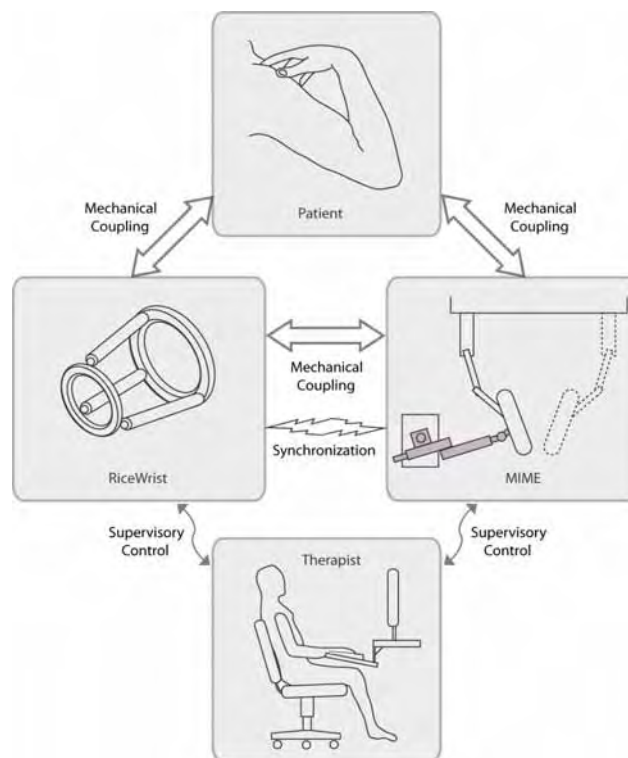Fig. 15. Subject operating the integrated MIME-*RiceWrist* System.

Fig. 16. MIME-*RiceWrist* rehabilitation system setup.

A graphical user interface (GUI), as shown in Fig. 17, is provided to the therapist to facilitate customization of the sessions. The GUI provides an interface to record patient information and individual session details. Prior to a therapy session, the therapist can record the joint limits of the patient to plan the desired start and end positions for reaching movements. This information is also stored on a local file for future reference and updates. For each trial, the therapist can then choose the desired trajectory by selecting start and end positions, number of repetitions and the speed of travel. Three different modes of operation — passive, triggered and constrained — are implemented on the system. Through the GUI, the therapist can also select the mode of operation and associated parameters.
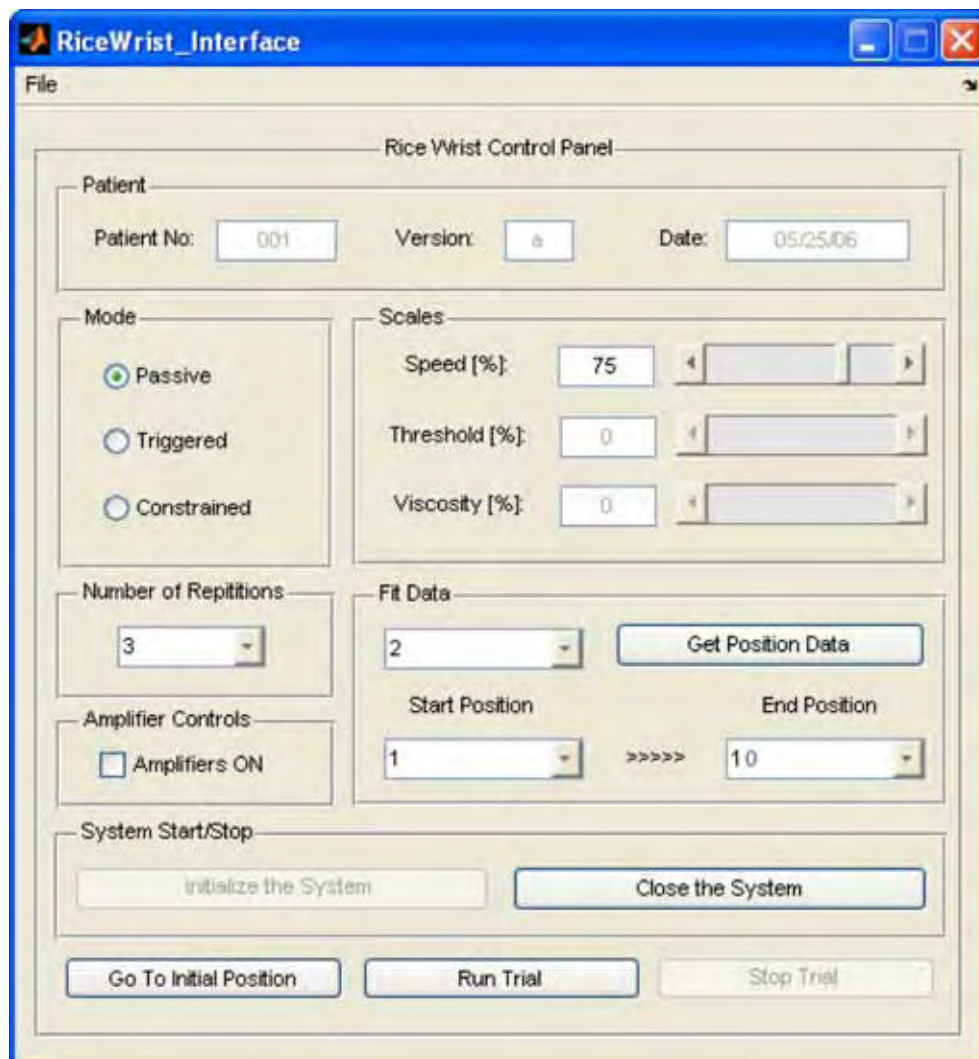

Fig. 17. Graphical user interface for the therapist

5.2 Control Modes

Three control modes that match the control modes of the MIME system — passive, triggered or constrained, have been implemented on the *RiceWrist*. Figure 18 depicts the structure of the controller for the MIME-*RiceWrist* system. The system has five modes of operation, three of which are the aforementioned control modes. The other modes are GoTo and Wait. When operating in the GoTo mode, the system moves to an initial position, which is specified by the therapist. On reaching the desired position, the system switches to the Wait mode, in which a virtual fixture is used to restrict arm movement, until the therapist initiates or resumes the trial. Following the command from the therapist, the system switches to one of the three control modes until the desired end position for the trial is reached. Upon reaching this position, the system switches back to the Wait mode until the therapist commands to initiate the return motion. This process can be repeated for the desired number of repetitions. The **GoTo mode** is implemented as a joint-space trajectory controller, as described in section 4.1. The desired trajectory is computed through linear interpolation using the current and specified initial positions. The **Wait mode** is implemented as a task-space impedance force controller. A high stiffness virtual wall prevents arm motions until a new mode is activated. **Passive** and **Triggered** modes are also implemented through joint-space controllers, whereas the **Constrained mode** is implemented as a task-space impedance force controller as used for the Wait mode. Unlike the Passive and Triggered modes, which are passive, this is an active mode where the patient is required to actively move his arm to the end position. Once movement has been initiated along the trajectory motion reversal is restricted by implementation of a virtual wall in that direction. Resistive impedance can also be displayed to the patient along the trajectory to provide strength training.
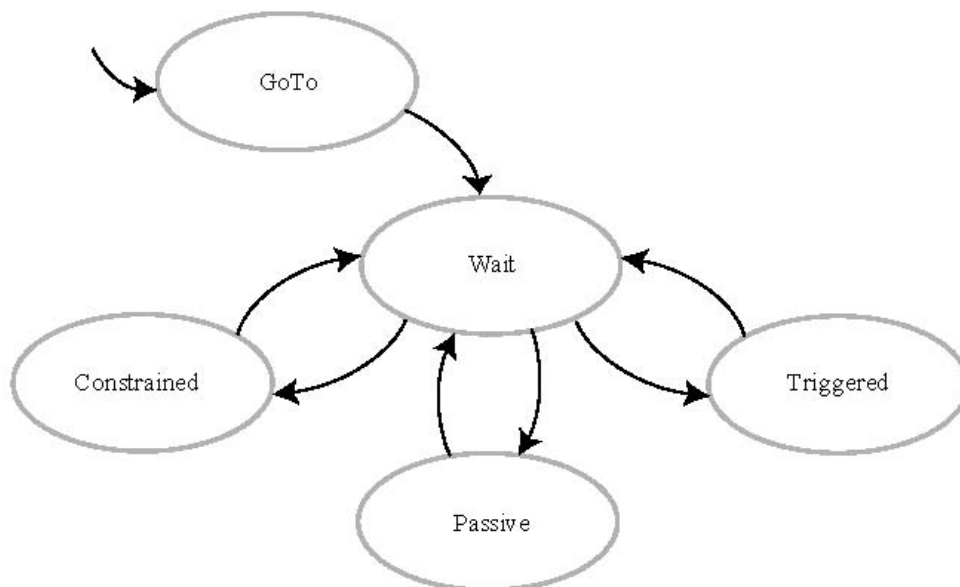

Fig. 18. Structure of the switching controller for the MIME-*RiceWrist* System.

5.3 Controller Performance of the *RiceWrist*

Figure 19 presents the experimental results when the *RiceWrist* is operating in the Passive Mode. Subfigures 19 (a)−(d) depict the trajectories for the four different joints, namely the wrist axes I, II, III, and forearm. Passive mode employs decoupled joint level trajectory controllers for each actuated axis. The solid lines in the figures represent the desired (commanded) trajectories, which are computed through linear interpolation between the specified initial and final joint positions. The dashed lines represent the experimentally recorded trajectories when the *RiceWrist* is operating freely. Finally, the dotted lines represent the experimentally recorded trajectories when the *RiceWrist* is worn by a human subject. The close match among the desired and experimentally observed trajectories imply adequate disturbance rejection characteristics of the implemented controllers.
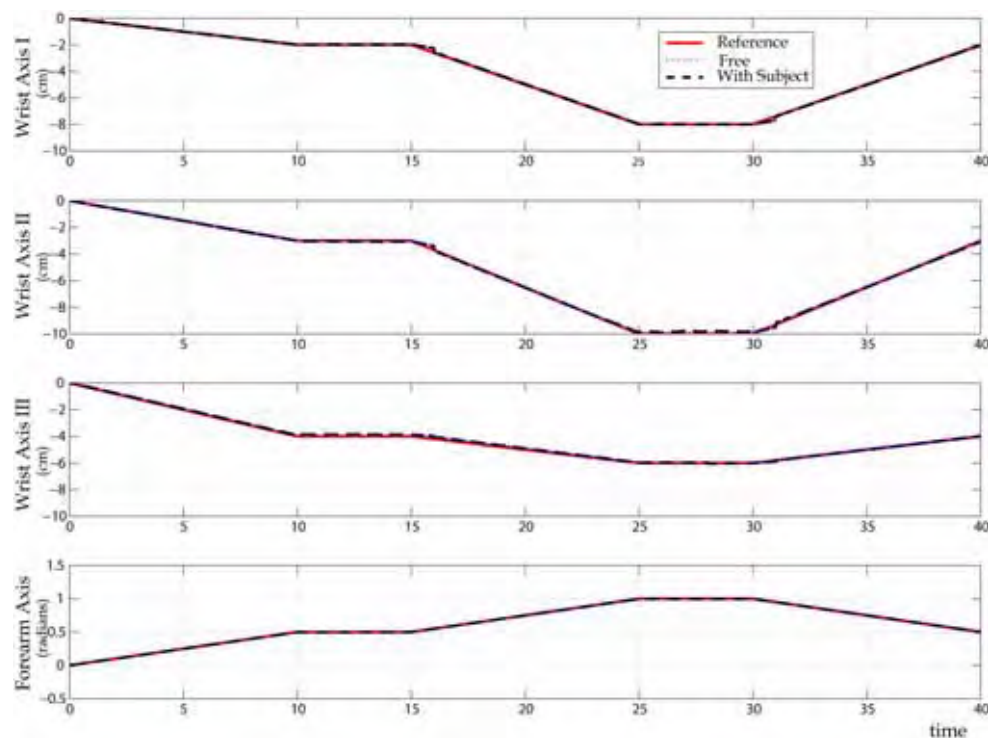

Fig. 19. Experimental results for the *RiceWrist* operating in the Passive mode.

6. Conclusions and Future work

This chapter has presented an overview of existing arm exoskeleton robotic devices, with a focus on those aimed at upper-extremity rehabilitation. The design and control of the MAHI arm exoskeleton was presented as a case study in exoskeleton design for rehabilitation applications. The device is compact, low-friction and backlash-free with high manipulability in the workspace of interest. Additionally, the MAHI exoskeleton allows unconstrained human arm movements over a large workspace and provides for

easy measurement of elbow, forearm and wrist joint angles. The device exhibits excellent behavior under position control with a fast response time, very small oscillations, little overshoot and small steady state errors. Furthermore, there is little structural coupling between various controlled degrees-of-freedom of the device (forearm rotation, wrist flexion/extension and wrist abduction/adduction). The ability of the device to independently provide accurate guidance or kinesthetic feedback to individual human joints is critical during motor learning. It is demonstrated that the device is able to simulate sufficiently stiff virtual surfaces although, the quality of the surface is limited by maximum torque output of the robot.

The chapter concludes by presenting the *RiceWrist*, a sub-set of the MAHI exoskeleton identical in design yet lacking the elbow joint, which has been integrated with the Mirror-Image Motion Enabler (MIME). The *RiceWrist* extends the three unilateral operation modes of MIME to include forearm supination and pronation, wrist flexion and extension, and radial and ulnar deviation. Currently, preliminary trials with healthy patients are underway in order to tune the experimental protocols of the MIME- *RiceWrist* system. Future work will focus on clinical trials with hemiparetic stroke patients to study the efficacy of the approach in forearm/wrist rehabilitation. The device will also be used as a test bed for studying mechanisms of human motor learning and development of training methodologies.

7. References

Basdogan, C., C.-H. Ho, et al. (2001). "Virtual Environments for Medical Training: Graphical and Haptic Simulation of Laproscopic Common Bile Duct Exploration." *IEEE/ASME Trans. Mechatron.* **6**(3): 269-285.

Bergamasco, M., B. Allotta, et al. (1994). *An Arm Exoskeleton System for Teleoperation and Virtual Environment Applications*. IEEE Int'l Conf. Robot. Automat.

Boman, D. K. (1995). "International Survey: Virtual-Environment Research." *Computer* **28** (6): 57-65.

Burdea, G. C. (1996). *Force and Touch Feedback for Virtual Reality*, John Wiley Inc.

Burgar, C. G., P. S. Lum, et al. (2000). "Development of Robots for Rehabilitation Therapy: The Palo Alto VA/Stanford Experience." *Journal of Rehabilitation Research and Development* **37**(6): 663-673.

Carignan, C. and M. Liszka (2005). *Design of an arm exoskeleton with scapula motion for shoulder rehabilitation*. IEEE Conference on Advanced Robotics.

Carignan, C. R. and D. L. Akin (2003). Using Robots for Astronaut Training. *IEEE control syst. mag.* **23:** 46-59.

Charles, S. K. K., H. I.; Volpe, B. T.; Lynch, D. & Hogan, N. (2005). *Wrist Rehabilitation Following Stroke: Initial Clinical Results*. International Conference on Rehabilitation Robotics.

Colgate, J. E. and J. M. Brown (1994). *Factors Affecting the Z-Width of a Haptic Display*. IEEE Int'l Conf. Robot. Automat.

Dirette, D. and J. Hinojosa (1994). "Effects of Continuous Passive Motion on the Edematous Hands of Two Persons with Flaccid Hemiplegia." *American Journal of Occupational Therapy* **48**(5): 403-409.

Elllis, R. E., O. M. Ismaeil, et al. (1996). "Design and Evaluation of a High-Performance Haptic Interface." *Robotica* **14**: 321-327.

Erlandson, R. F. (1992). "Applications of Robotic/Mechatronic Systems in Special Education, Rehabilitation Therapy." *IEEE Trans. Rehab. Eng.* **3**(1): 22-34.

Fasoli, S. E., H. I. Krebs, et al. (2004). "Robotic Technology and Stroke Rehabilitation." *Topics in Stroke Rehabilitation* **11**: 11-19.

Feygin, D., M. Keehner, et al. (2002). *Haptic Guidance: Experimental Evaluation of a Haptic Training Method for a Perceptual Motor Skill*. Int'l Sympo. Haptic Interfaces for Virtual Environ. Teleop. Syst.

Gillespie, B., S. O'Modhrain, et al. (1998). *The Virtual Teacher*. ASME Int'l Mech. Eng. Congress Expo.

Goodall, R. M., D. J. Pratt, et al. (1987). "Enhancing Postural Stability in Hemi-Plegics Using Externally Applied Forces." *Intl. J. of Rehab. Research (suppl 5)* **10**(4): 132-140.

Gresham, G. E. (1990). "Past Achievements and New Directions in Stroke Outcome Research." *Stroke* **21 (9 Suppl):II**: 1-2.

Gresham, G. E., D. Alexander, et al. (1997). "Rehabilitation." *Stroke* **28**(7): 1522-1526.

Gupta, A. and M. K. O'Malley (2006). "Design of a Haptic Arm Exoskeleton for Training and Rehabilitation." *IEEE/ASME Trans. Mechatron.* **11**(3).

Gupta, A., V. Patoglu, et al. (2007). "Design, Control and Performance of RiceWrist: A Force Feedback Wrist Exoskeleton for Rehabilitation and Training." *Int'l J. Robot. Research*.

Hesse, S., G. Schulte-Tigges, et al. (2003). "Robot Assisted Arm Trainer for the Passive and Active Practice of Bilateral Forearm and Wrist Movements in Hemiparetic Subjects." *Archives of Physical Medicine and Rehabilitation* **84**(6): 915-920.

Hogan, N. and H. I. Krebs (2004). "Interactive Robots for Neurorehabilitation." *Restorative Neurology and Neuroscience* **22**: 349-358.

Jack, D., R. Boian, et al. (2001). "Virtual Reality Enhanced Stroke Rehabilitation." *IEEE Trans. Neural Syst. Rehab. Eng.* **9**(3): 308-318.

Jeong, Y., Y. Lee, et al. (2001). *A 7 DOF Wearable Robotic Arm using Pneumatic Actuators*. Int'l Symp. Robot.

Khalili, D. and M. Zomlefer (1988). "An Intelligent Robotic System for Rehabilitation of Joints and Estimation of Body Segment Parameters." *IEEE Trans. Biomed. Eng.* **35**(2): 138-146.

Kim, Y. S., J. Lee, et al. (2005). "A force Reflected Exoskeleton-Type Masterarm for Human-Robot Interaction." *IEEE Trans. Syst., Man, Cybern. A* **35**(2): 198-212.

Kousidou, S., N. Tsagarakis, et al. (2006). *Assistive Exoskeleton for Task Based Physiotherapy in 3-Dimensional Space*. IEEE/RAS-EMBS International Conference on Biomedical Robotics and Biomechatronics.

Lay, S. D. and A. M. Day (2003). "Recent Developments and Applications of Haptic Devices." *Comp. Graph. Forum* **22**(2): 117-132.

Lee, K. M. and D. K. Shah (1988). "Kinematic Analysis of a Three Degrees-of-Freedom in-Parallel Actuated Manipulator." *IEEE Trans. Robot. Automat.* **4**(3): 354-360.

Lee, S., S. Park, et al. (1998). *Design of a Force Reflecting Master Arm and Master Hand using Pneumatic Actuators*. IEEE Int'l Conf. Robot. Automat.

Mosher, R. S. (1967). From Handyman to Hardiman, SAE paper no.670088.

Nakai, A., T. Oshashi, et al. (1998). *7DOF Arm Type Haptic Interface for Teleoperation and Virtual Reality Systems*. Int'l Conf. Intell. Robots Syst.

Nef, T., M. Mihelj, et al. (2006). *ARMin – Robot for Rehabilitation of the Upper Extremities*. IEEE International Conference on Robotics and Automation.

O'Malley, M. K. and M. Goldfarb (2002). "The Effect of Force Saturation on the Haptic Perception of Detail." *IEEE/ASME Trans. Mechatron.* **7**(3): 280-288.

O'Malley, M. K. and M. Goldfarb (2004). "The Effect of Virtual Surface Stiffness on the Haptic Perception of Detail." *IEEE/ASME Trans. Mechatron.* **9**(2).

O'Malley, M. K. and A. Gupta (2003). *Passive and Active Assistance for Human Performance of a Simulated Underactuated Dynamic Task*. Int'l Sympo. Haptic Interfaces for Virtual Environ. Teleop. Syst.

O'Malley, M. K., T. Ro, et al. (2006). "Assessing and Inducing Neuroplasticity with TMS and Robotics." *Archives of PMR, Special Issue on Neuroplasticity and Neuroimaging in Acquired Brain Injury: Measurements, Concepts, and Applications*.

Perry, J. C. and J. Rosen (2006). *Design of a 7 Degree-of-Freedom Upper-Limb Powered Exoskeleton*. IEEE Conference on Biomedical Robotics and Biomechatronics.

Prisco, G. M., C. A. Avizzano, et al. (1998). *A Virtual Environment with Haptic Feedback for the Treatment of Motor Dexterity Disabilities*. IEEE Int'l Conf. Robot. Automat.

Reinkensmeyer, D. J., J. P. A. Dewald, et al. (1996). "Robotic Devices for Physical Rehabilitation of Stroke Patients: Fundamental Requirements, Target Therapeutic Techniques, and Preliminary Designs." *Technology and Disability* **5**: 205-215.

Reinkensmeyer, D. J., J. L. Emken, et al. (2004). "Robotics, Motor Learning and Neurologic Recovery." *Annual Reviews in Biomedical Engineering* **6**: 497-525.

Reinkensmeyer, D. J., C. D. Takahashi, et al. (2000). "Design of Robot Assistance for Arm Movement Therapy Following Stroke." *Advanced Robotics* **14**(7): 625-637.

Riener, R., T. Nef, et al. (2005). "Robot-Aided Neurorehabilitation of the Upper Extremeties." *Medical and Biological Engineering and Computing* **43**: 2--10.

Rosen, J., M. Brand, et al. (2001). "A Myosignal-Based Powered Exoskeleton System." *IEEE Trans. Syst., Man, Cybern. A* **31**(3): 210--222.

Rosenberg, L. (1993). *Virtual Fixtures: Perceptual Tools for Telerobotic Manipulation*. IEEE Int'l Symp. Virt. Reality.

Ruiz, A. F., A. Forner-Cordero, et al. (2006). *Exoskeletons for Rehabilitation and Motor Control*. Biomedical Robotics and Biomechatronics, 2006. BioRob 2006. The First IEEE/RAS-EMBS International Conference on.

Shimoga, K. (1992). *Finger Force and Touch Feedback Issues in Dexterous Telemanipulation*. NASA-CIRSSE Int'l Conf. Intel. Robot. Syst. for Space Expl.

Sledd, A. and M. K. O'Malley (2006). *Performance Enhancement of a Haptic Arm Exoskeleton*. Int'l Sympo. Haptic Interfaces for Virtual Environ. Teleop. Syst.

Stein, J. (2004). "Motor Recovery Strategies after Stroke." *Topics in Stroke Rehabiliation* **11**: 12-22.

Sveistrup, H. (2004). "Motor Rehabilitation using Virtual Reality." *J. NeuroEng. and Rehab.* **1**(10).

Thom, T., N. Haase, et al. (2006). "Heart disease and stroke statistics-2006 update: a report from the American Heart Association Statistics Committee and Stroke Statistics Subcommittee." *Circulation* **113**(6): e85-151.

Todorov, E., R. Shadmehr, et al. (1997). "Augmented Feedback Presented in a Virtual Environment Accelerates Learning of a Difficult Motor Task." *J. Motor Behav.* **29**(2): 147-158.

Tsagarakis, N., D. G. Caldwell, et al. (1999). *A 7DOF Pneumatic Muscle Actuator Powered Exoskeleton*. Int'l Workshop Robot and Human Interact. Commun.

White, C. J., A. M. Scneider, et al. (1993). *Robotic Orthosis for Stroke Patient Rehabilitation*. IEEE Intl. Conf. Eng. Med. Biol.

Williams II, Robert L.; Murphy, Mark A.; North, Debra; Berlin, James & Krier, Michael (1998). *Kinesthetic Force/Moment Feedback via Active Exoskeleton*. Image Society Conf.

Wolf, P. A., R. B. D'Agostino, et al. (1992). "Secular Trends in Stroke Incidence and Mortality: The Framingham Study." *Stroke* **23**: 1551--1555.

Yoshikawa, T. (1985). "Manipulability of Robotic Mechanisms." *Int'l J. Robot. Research* **4**(2): 3-9.